# Antimicrobial magnetic *Glycyrrhiza glabra* nanocomposite for decolouration of water through adsorption and photodegradation

Ankita Manchanda[1], Ahmed Hussain Jawhari[2], Ziaul Hasan[3], Nazim Hasan[2,4], Sneha Shukla[1], Adiba Khan[1], Tabrez Alam Khan[1], Saif Ali Chaudhry[1]*
[1]Department of Chemistry, Jamia Millia Islamia, New Delhi-110025, India
[2]Department of Physical Sciences, Chemistry Division, College of Science, Jazan University, P.O. Box. 114, Jazan-45142, Kingdom of Saudi Arabia
[3]Department of Biosciences, Jamia Millia Islamia, New Delhi-110025, India
[4]Nanotechnology Research Unit, Jazan University, P.O. Box 114, Jazan 45142, Saudi Arabia
Corresponding E-mail: schaudhry@jmi.ac.in **(Saif A Chaudhry)**

## Supplementary Information

### Debye-Scherrer equation

The estimation of average crystallite grain size (D, nm) of GG/γ-$Fe_2O_3$ NPs from the full width at half maximum (FWHM) using Debye-Scherrer equation was performed using the given equation:

$$D = \frac{K\,\lambda}{\beta\,Cos\theta} \quad \text{(S1)}$$

where, λ is wavelength of incident X-ray radiation (λ = 0.154 nm), K is the Scherrer constant (=0.9 for cubic shape), θ is Bragg's angle of diffraction (radians), while β corresponds to FWHM (radians).

### Zero-point charge of GG/γ-$Fe_2O_3$

The amount and nature of charge acquired by the solid surface directly correlates to the presence of $H^+$ and $OH^-$ in the aqueous dispersion phase, which either protonate or deprotonate the surface functional groups (MOH/MCOOH). This amphoteric behaviour of functional groups paves way for the development of either positive or negative charge on the solid surface above and below the neutral zero-point charge, ZPC condition as indicated below.

Protonation at low pH:

$$MOH\,(surface) + H^+(aq) \rightarrow MOH_2^+\ \text{(surface)}$$

$$MCOOH(surface) + H^+(aq) \rightarrow MCOOH_2^+\ \text{(surface)}$$

Deprotonation at high pH:

$$MOH\,(surface) + OH^-(aq) \rightarrow MO^-(surface) + H_2O(l)$$

$$MCOOH\,(surface) + OH^-(aq) \rightarrow MCOO^-(surface) + H_2O\,(l)$$

At ZPC, there is an equal concentration of both $MOH_2^+$ / $MCOOH_2^+$ and $MO^-$ / $MCOO^-$ species on the GG/γ-$Fe_2O_3$ surface, hence the total net electric charge density equilibrates to zero. During adsorption, the ZPC controls the ionic interaction between the surface functional active

sites and cationic (NB) and anionic (CR) dyes that adhere onto these sites, regulating the effect of change in pH of aqueous solution on the latter, as shown below.

For anionic dye Congo red (CR):

$$MOH_2^+(surface) + CR^-(aq) \rightarrow MOH_2^+ CR^- (surface)$$

$$MCOOH_2^+(surface) + CR^-(aq) \rightarrow MCOOH_2^+ CR^- (surface)$$

For cationic dye Nile blue (NB):

$$MOH_2^+(surface) + NB^+(aq) \rightarrow MO^- NB^+(surface) + 2H^+(aq)$$

$$MCOOH_2^+(surface) + NB^+(aq) \rightarrow MCOO^- NB^+(surface) + 2H^+(aq)$$

For GG/γ-$Fe_2O_3$ surface, ZPC was found to be 6.9 (Fig. S5), and above and below pH 6.9, the surface acquired charge.

**Thermodynamics of adsorption process**

The adsorption data obtained at 30, 40, and 50 °C was substituted in the below stated thermodynamic equations to compute ΔG [**Eq. S2**], ΔH (slope of $log\left(\frac{Q_e}{C_e}\right)$ vs. 1/T plot), and ΔS (intercept of $log\left(\frac{Q_e}{C_e}\right)$ vs. 1/T plot) [**Eq. S3**].

$$\Delta G = -RT\ ln\ K_C \quad (S2)$$

$$log\left(\frac{Q_e}{C_e}\right) = \frac{\Delta S}{2.303R} - \frac{\Delta H}{2.303RT} \quad (S3)$$

where T is absolute temperature, $K_c$ (= $Q_e/C_e$), is the equilibrium constant, and R (= 0.008314 $kJmol^{-1}K^{-1}$) is the universal gas constant.

**Webber-Morris Intraparticle diffusion (IPD)**

The solute uptake is in proportion with time and expressed as:

$$Q_t = k_{IPD} t^{0.5} + C \quad (S4)$$

The equation produces a linear plot between $Q_t$ and $t^{0.5}$, the slope of which determines the IPD rate constant, $k_{IPD}$ ($mgg^{-1}min^{-0.5}$) (**Table S6**). If the experimental data fits well in the above equation producing a straight-line plot passing through origin, then IPD would be the rate limiting step, otherwise the kinetics is governed by the film diffusion model. However, intercept, C, incorporates partial film diffusion driven rate kinetics since both processes might occur simultaneously. Moreover, the intercept value provides a fair idea of the thickness of the boundary layer.

**Boyd's-Liquid film diffusion (LFD)**

$$-\ ln\,(1\ -\ F)\ =\ k_{LFD}t \qquad \text{(S5)}$$

where, $k_{LFD}$ ($min^{-1}$) is the film diffusion rate constant, while F (= $Q_t/Q_e$) depicts the fraction of pollutant ions adsorbed time t. If on plotting -ln (1-F) against t, a straight line is obtained with slope $k_{LFD}$ that passes through origin, then the adsorption kinetics obey the LFD model.

**Supplementary Figures:**

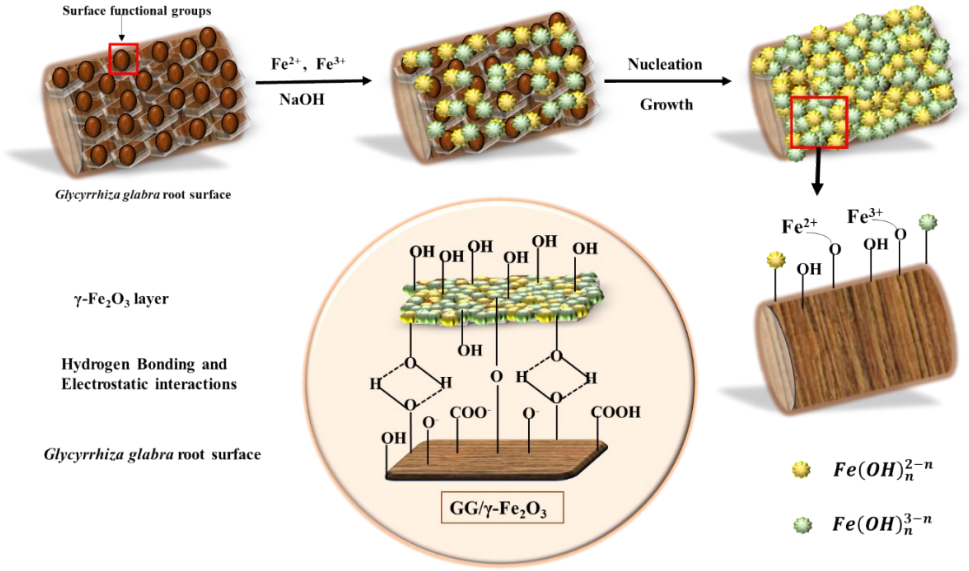


**Fig. S1:** Pictorial representation of interactions leading to the formation of GG/γ-$Fe_2O_3$

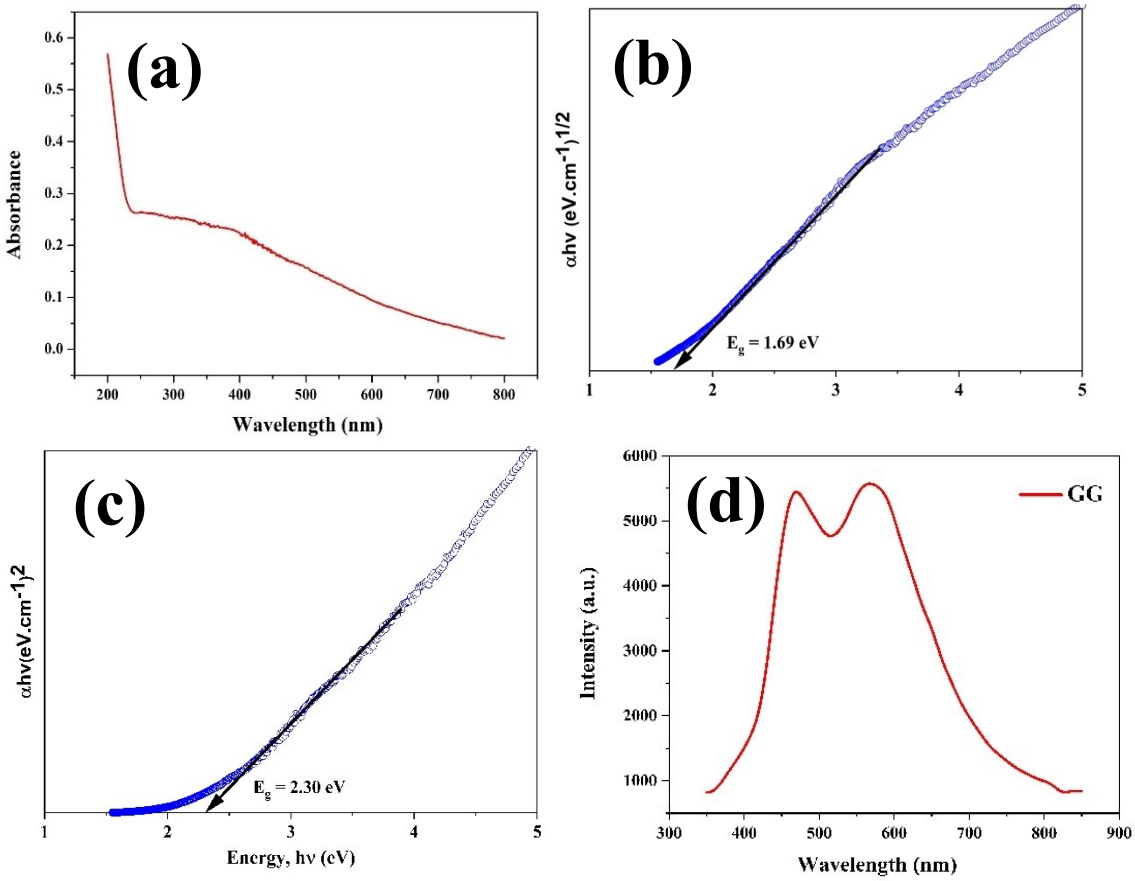

**Fig. S2:** (a) UV-Visible; (b) Indirect, and (c) Direct Tauc plot of GG/γ-$Fe_2O_3$; (d) PL spectra of GG

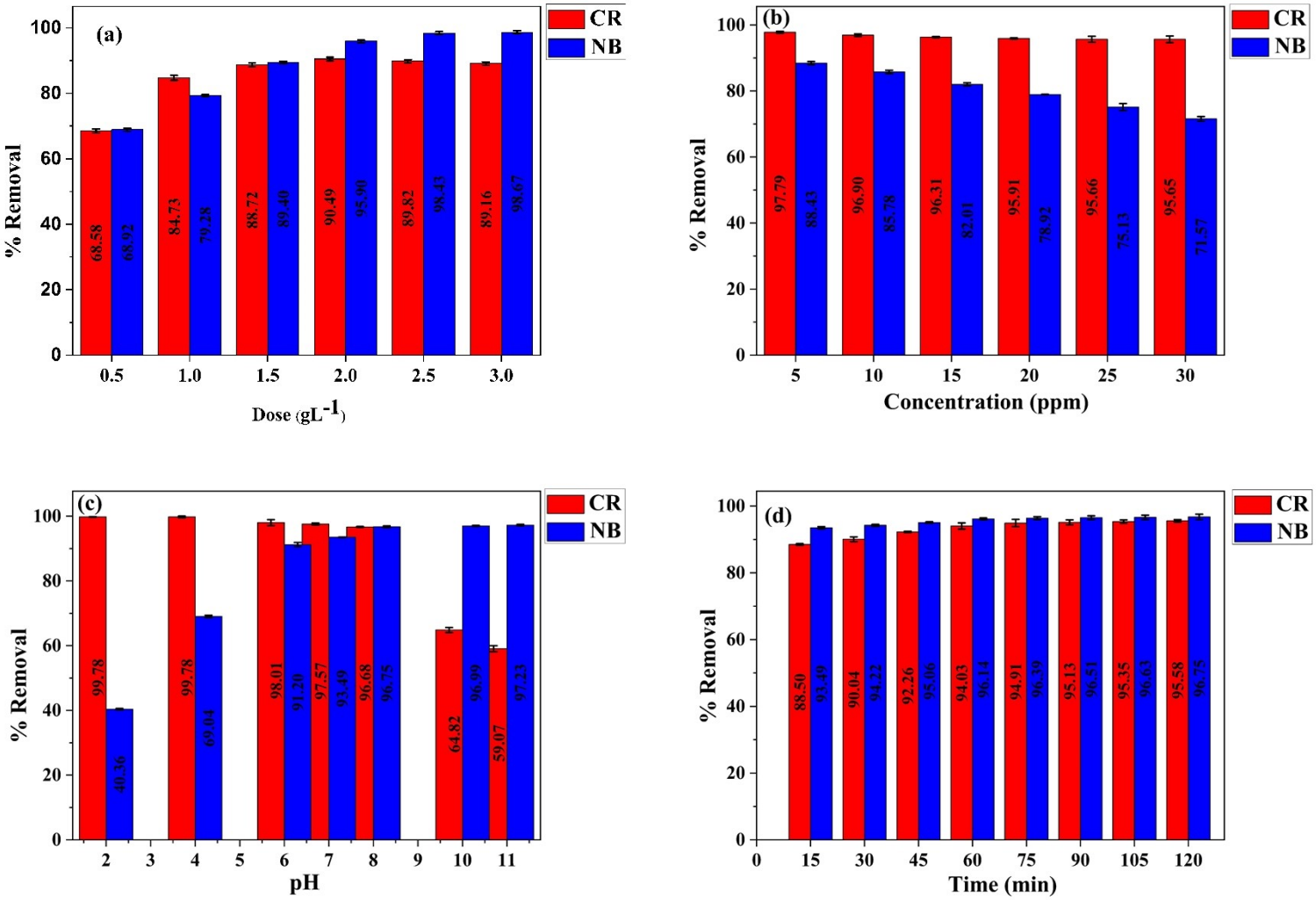


**Fig. S3:** Effect of operative variables on removal of CR and NB dyes, (a) Dosage of GG/γ-$Fe_2O_3$, (b) Concentration of dyes, (c) pH and (d) Time of equilibration

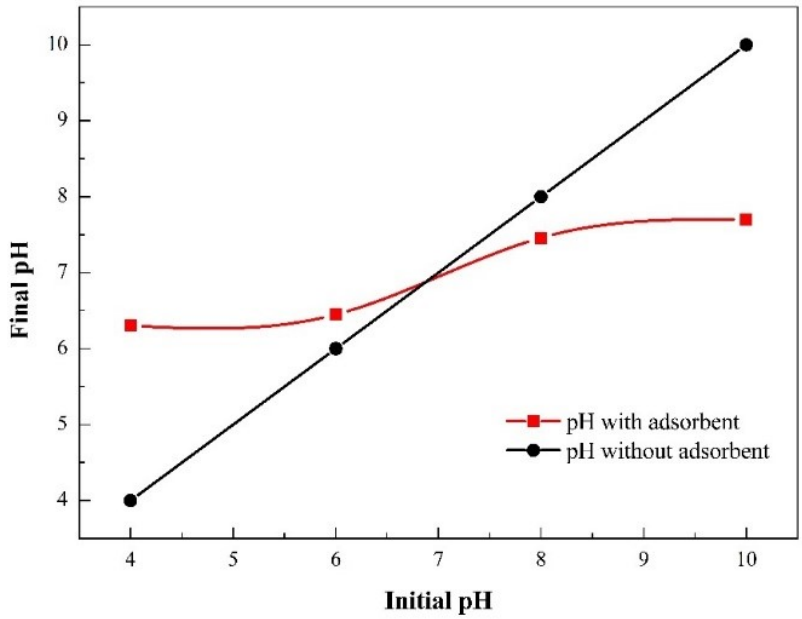


**Fig. S4:** Zero-point charge of GG/γ-$Fe_2O_3$

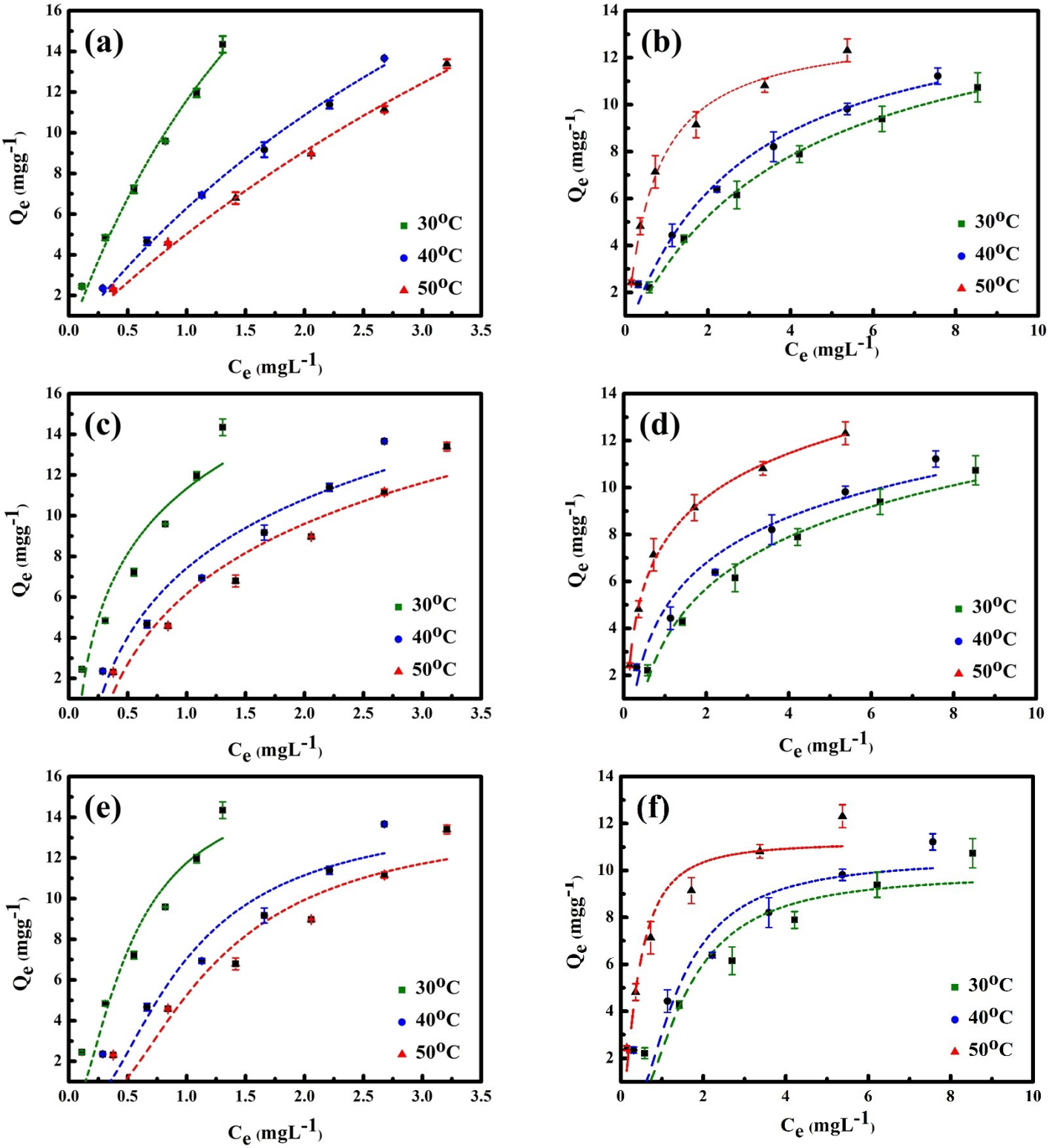


**Fig. S5:** Non-linear (a) Langmuir, (c) Temkin, and (e) Dubinin-Radushkevich isotherms for CR adsorption; (b) Langmuir, (d) Temkin, and (f) Dubinin-Radushkevich isotherms for NB adsorption

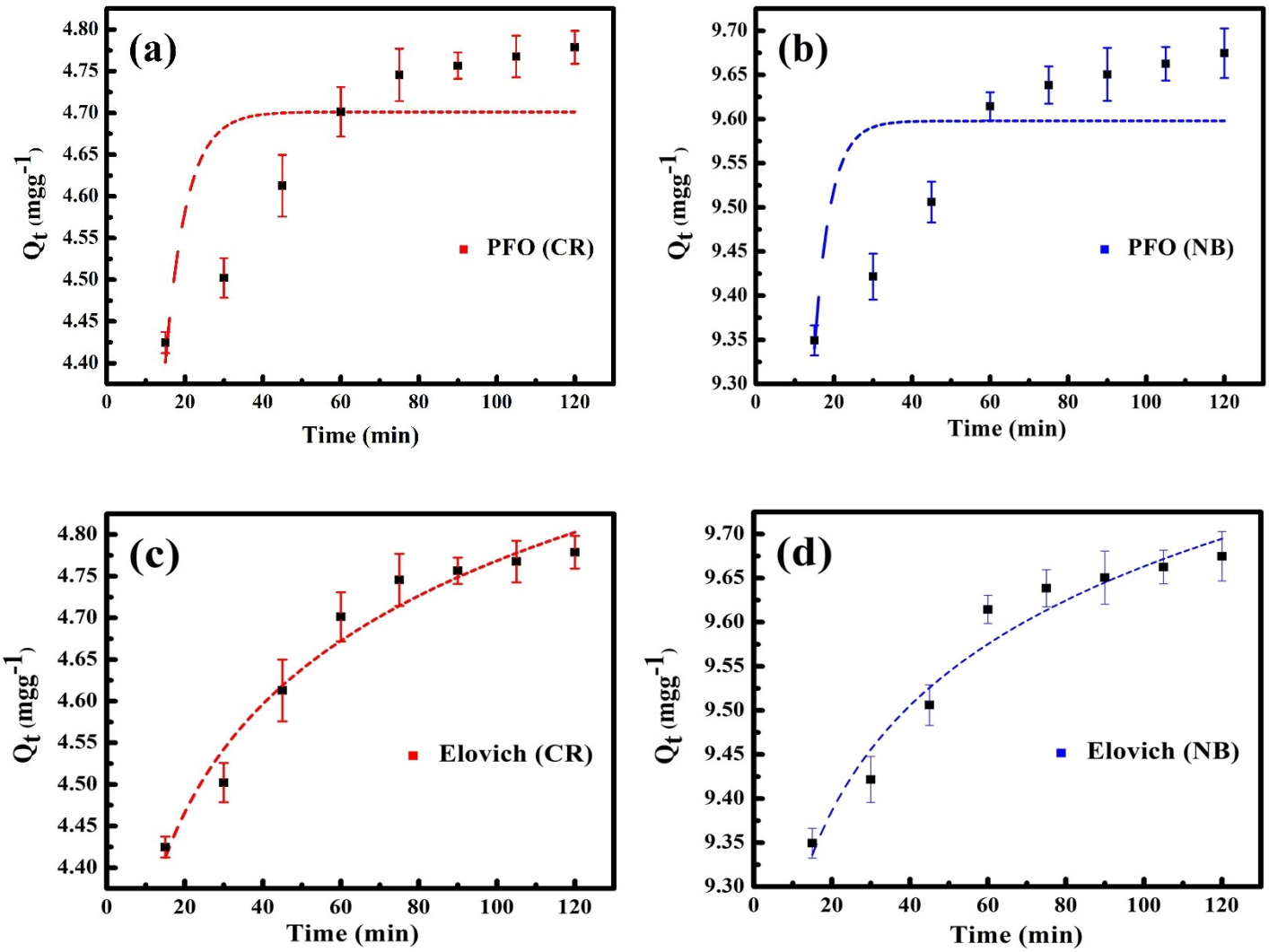


**Fig. S6:** Non-linear (a) Pseudo-first order (PFO) and (c) Elovich plots for CR adsorption; (b) Pseudo-first order (PFO) and (d) Elovich plots for NB adsorption

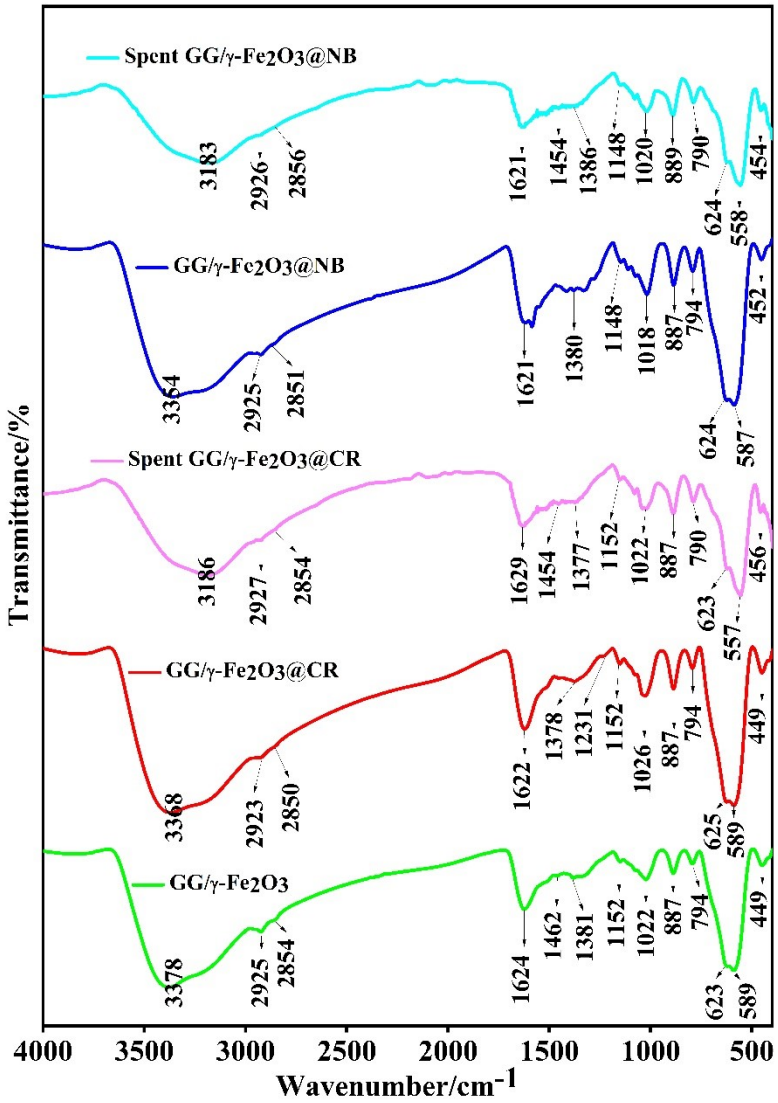


**Fig. S7.** FT-IR spectra of GG/γ-$Fe_2O_3$ before and after CR/NB adsorption, and of spent GG/γ-$Fe_2O_3$ after desorbing CR/NB dyes

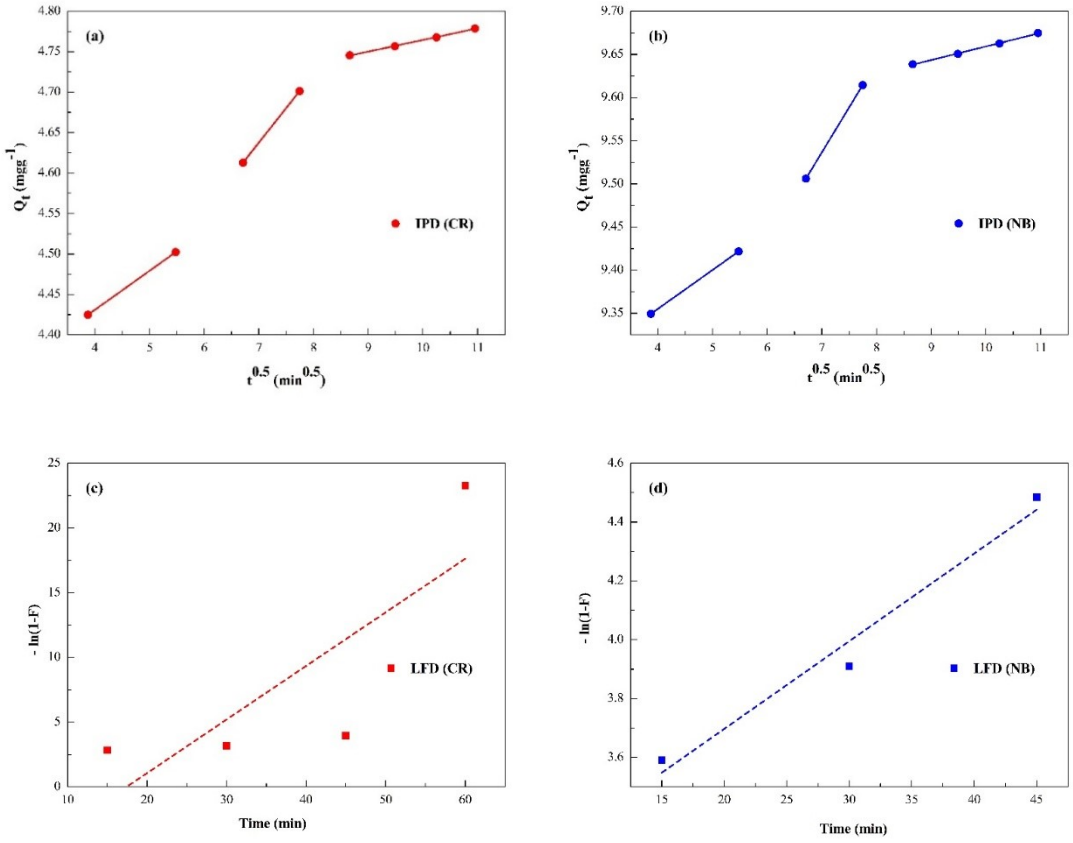


**Fig. S8:** (a) and (b) depicts Webber-Morris/ Intra-particle diffusion (IPD) model, and (c) and (d) depicts Liquid film diffusion model (LFD) for CR and NB sorption on GG/γ-$Fe_2O_3$, respectively

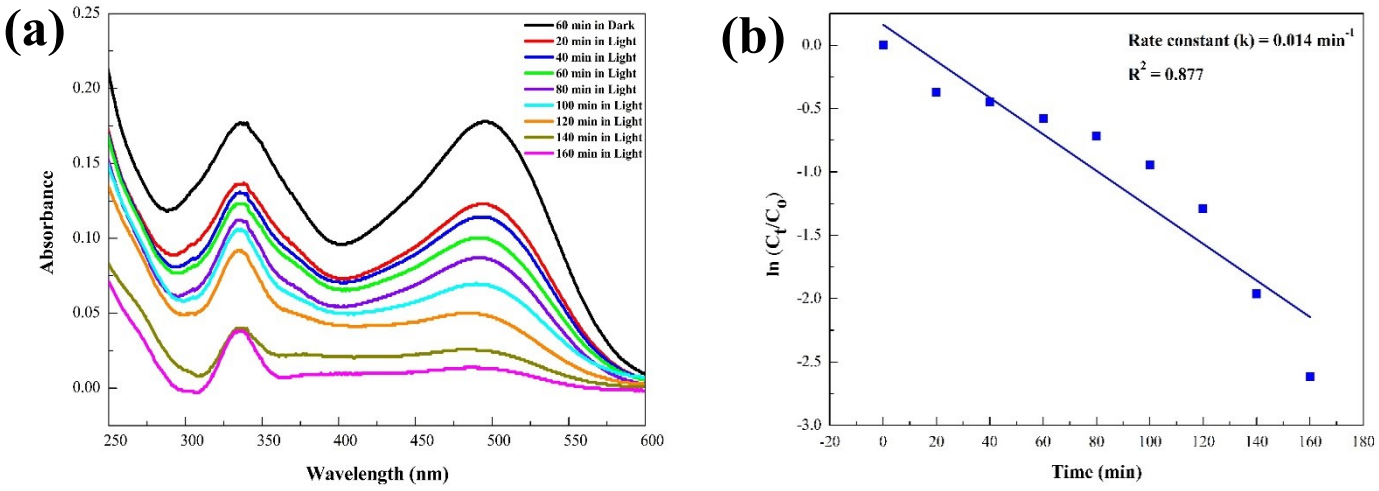


**Fig. S9:** (a) Time dependent UV-Visible absorption spectra, and (b) Pseudo-first order (PFO) kinetic plot for photodegradation of CR dye using GG/γ-$Fe_2O_3$

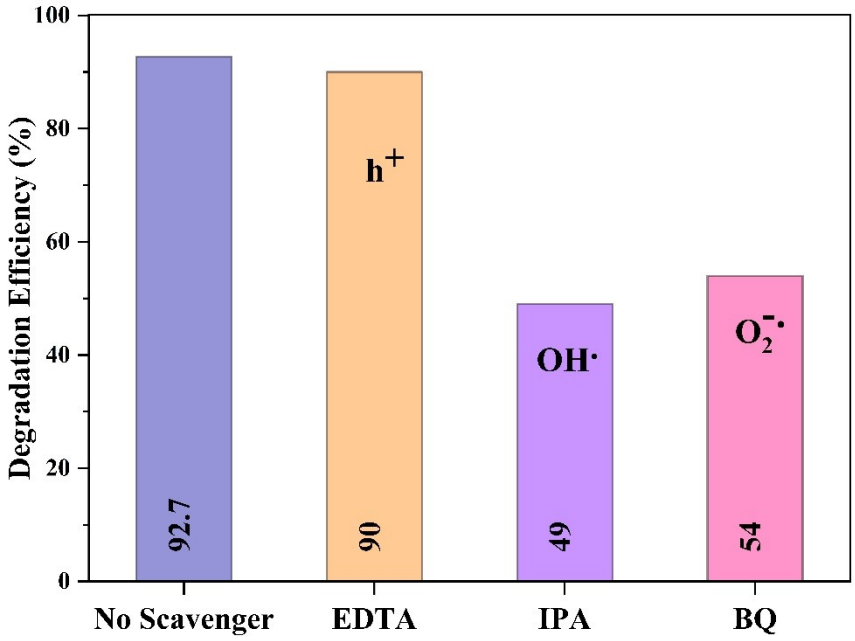


**Fig. S10.** Effect of radical scavengers on the photocatalytic degradation performance of GG/γ-$Fe_2O_3$

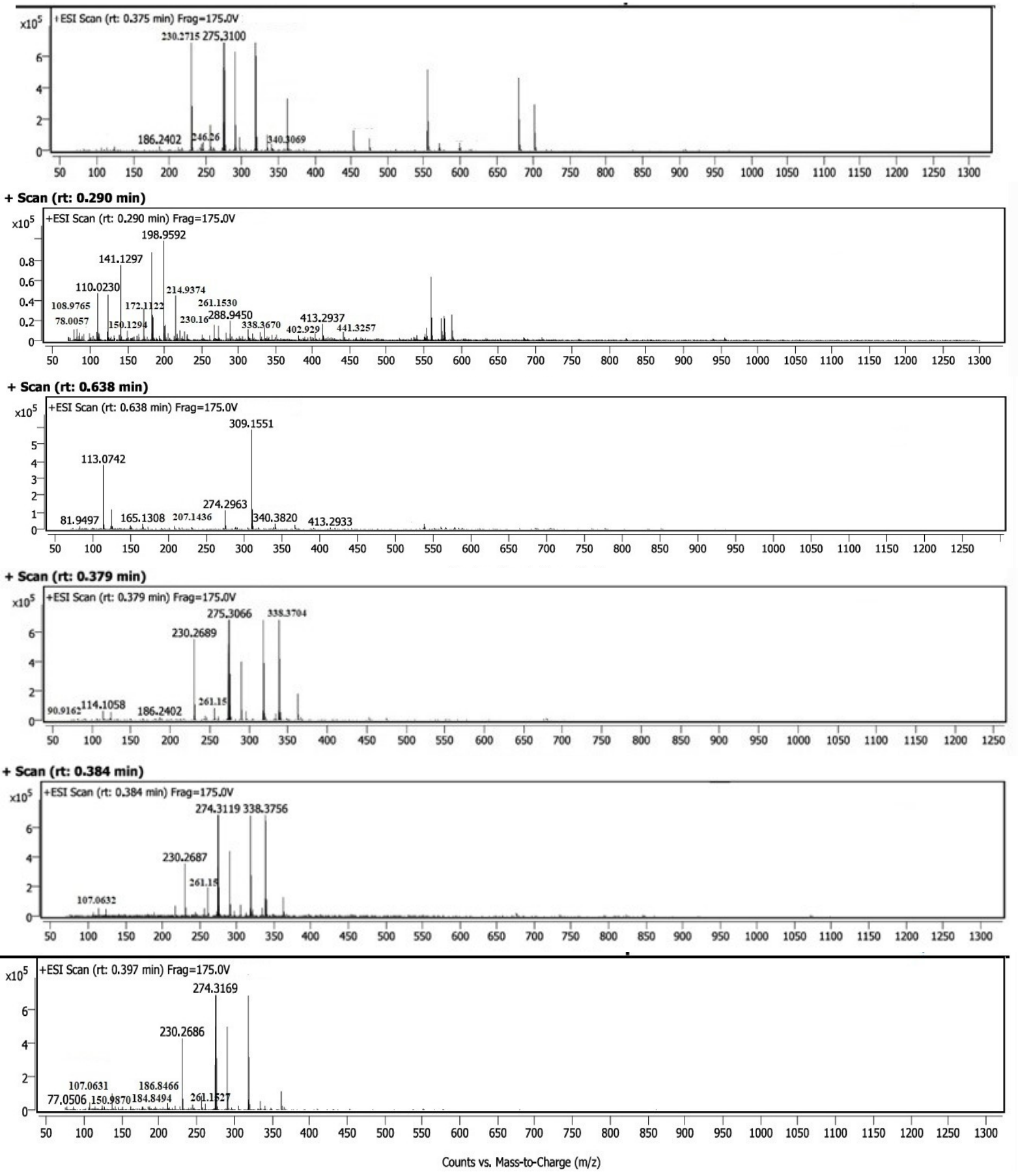


**Fig. S11.** Time resolved high resolution LC-HRMS mass spectra for CR degradation by

GG/γ-$Fe_2O_3$ at different time intervals

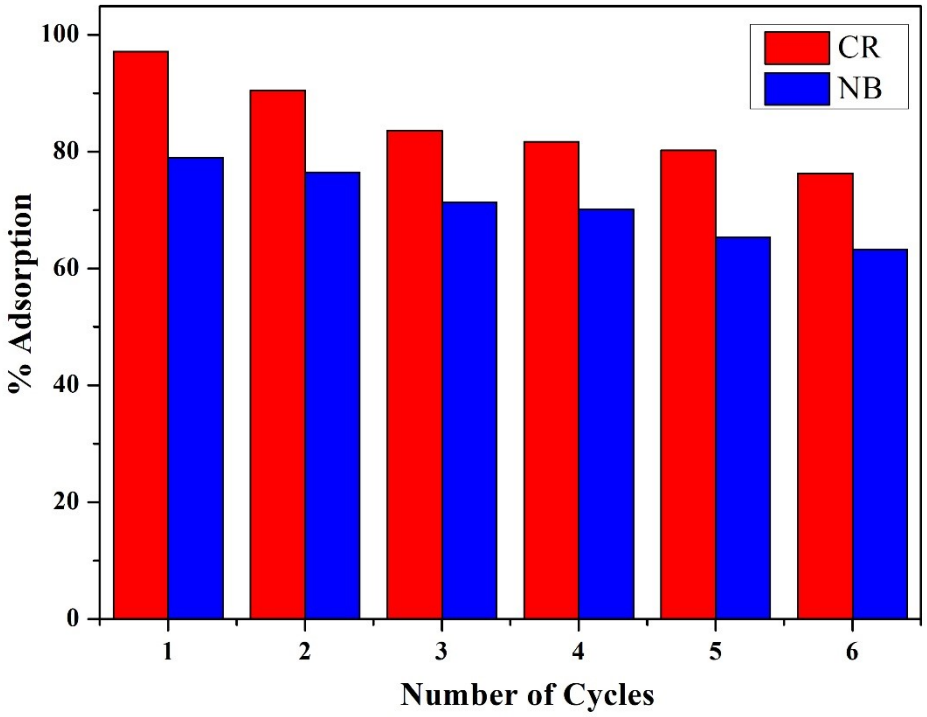


**Fig. S12.** Regeneration-reusability cycles of GG/γ-$Fe_2O_3$

**Supplementary Tables:**

**Table S1.** Chemicals utilised for the synthesis of GG/γ-$Fe_2O_3$

| **Chemicals/Reagents* (AR grade)/Materials** | **Purchased from** |
|---|---|
| *Glycyrrhiza glabra* plant roots | Local market in West Delhi, India |
| Ferrous sulphate heptahydrate {$FeSO_4.7H_2O$, minimum assay > 99.5%}, Calcium chloride dihydrate {≥ 98%}, Direct Red-81 {DR-81} | Merck India Ltd., New Delhi |
| Ferric nitrate nanohydrate {$Fe(NO_3)_3.9H_2O$, minimum assay 98%} | Thermo Fisher Scientific India Pvt. Ltd., New Delhi |
| Congo red {$C_{32}H_{22}N_6Na_2O_6S_2$, M.W.= 696.65gmol$^{-1}$, $\lambda_{max}$= 498 nm}, Isopropanol {IPA, min 99%}, Malachite green {MG}, Eosine yellow {EY}, New fuchsin {NF}, Thymol blue {TB}, Crystal violet {CV}, Phloxin B {Ph}, Chlorophenol red {Ch-R} | Loba Chemie Pvt., Ltd., India |
| Nile blue {$C_{20}H_{20}ClN_3O$, M.W.= 353.85 gmol$^{-1}$, $\lambda_{max}$= 627 nm} | HiMedia Laboratories Pvt. Ltd., India |
| Bismark brown-R {BB-R} | CDH (P) Ltd., India |
| Sodium hydroxide pellets {minimum assay > 97%}, Hydrochloric acid {minimum assay (alkalimetric) ≥ 32%}, and Potassium nitrate {minimum assay 99%, Sodium sulphate {minimum assay 99.5%, Sodium nitrate {minimum assay ≥ | Merck India Ltd., New Delhi |

| | |
|---|---|
| 99%}, Sodium chloride {minimum assay ≥ 99%}, Sodium carbonate {minimum assay ≥ 99.5%} | |
| Acetone {minimum assay > 99.5%, Alizarin red S {AR-S} | Fisher Scientific Ltd., India |
| EDTA {99%} | SRL Pvt. Ltd., India |
| 1,4-benzoquinone {BQ, 99%} | Ottokemi, India |
| Ethanol, Yeast extract, Peptone, Dextrose, Dimethyl sulphoxide (DMSO), and Agar | Sigma Chemical Co., St. Louis, MO, USA |
| Fungal strains of *Candida albicans* SC-5314 and ATCC-90028 | National Institute for Microbial Resource (NCMR), Pune, India |
| Bacterial strains of *Escherichia coli* (ATCC-25922) and *Staphylococcus aureus* (MTCC-902) | Institute of Microbial Technology (IMTECH), Chandigarh, India |

*All chemicals and reagents were used as obtained without any additional purification procedure. Doubly distilled water was used throughout the experiments.

**Table S2.** Characterization of GG/γ-$Fe_2O_3$

| **Characterization Technique** | **Sample(s)** | **Instrument Used** | **Range and Specifics** | **Information** |
|---|---|---|---|---|
| FT-IR | GG, GG/γ-$Fe_2O_3$, GG/γ-$Fe_2O_3$@CR, GG/γ-$Fe_2O_3$@NB | Perkin-Elmer spectrometer | 4000-400 $cm^{-1}$ using pellets in KBr | Specific interactions between metal oxide, GG and dyes, functional group analysis |
| | Spent GG/γ-$Fe_2O_3$@CR, Spent GG/γ-$Fe_2O_3$@NB | Nicolet iS50 | | |
| P-XRD | GG, GG/γ-$Fe_2O_3$ | Rigaku diffractometer | Continuous scanning angular range 05 to 90° (2θ), Cu-Kα radiation of λ=1.54 Å (40 kV, 30 mA) at RT | Crystal structure, phase and crystal size |
| FE-SEM | GG and GG/γ-$Fe_2O_3$ | Thermal field emission type Zeiss Gemini SEM 500 | 10-15 kV accelerating voltage | Morphological and microstructural investigation |
| HR FE-SEM | GG/γ-$Fe_2O_3$ and GG/γ-$Fe_2O_3$@CR | Nova Nano SEM-450, FEI, Netherlands | 10 kV | |
| EDX | GG and GG/γ-$Fe_2O_3$ | Thermal field emission type Zeiss Gemini SEM 500 microscope | 15 kV | Identification and mapping of elemental composition |
| TEM and SAED | GG/γ-$Fe_2O_3$ | F30 S-Twin, Tecnai microscope | - | Morphological and microstructural distribution of particles, and particle size |
| BET | GG/γ-$Fe_2O_3$ | Micromeritics' Gemini VII 2380 Series surface analyzer | $N_2$ adsorption-desorption isotherm | Surface area and porosity |

| | | | | |
|---|---|---|---|---|
| VSM | GG/γ-$Fe_2O_3$ | MicroSense, Model ADE-EV9 | -2 to +2 T | Magnetic property measurements |
| XPS | GG/γ-$Fe_2O_3$ | Thermo Scientific K-Alpha XPS System | 0-1350 eV; Al Kα source (hν = 1486.6 eV) | Elemental analysis and bonding interactions |
| TGA | GG/γ-$Fe_2O_3$ | TA TGA 5500 | $N_2$ atmosphere, 30-800° C, Heating Rate: 10°C$min^{-1}$ | Thermal stability |
| UV-Vis and CR degradation | GG/γ-$Fe_2O_3$ | UV-1800, Shimadzu UV-spectrophotometer | - | Band gap estimation |
| PL | GG, γ-$Fe_2O_3$, GG/γ-$Fe_2O_3$ | WiTech alpha 300R, Germany | Excitation λ = 325 nm (He-Cd laser) | Charge transfer efficiency, and rate of recombination |
| LC-HRMS | CR degradation intermediates | Agilent G6530AA (LC-HRMS-BIO-QTOF) | Source: ESI and APCI; HPLC pressure: 600 Bar, MS pressure: $10^{-4}$ to $10^{-5}$ Torr | CR degradation intermediates and byproducts |

**Table S3.** Standard deviation (SD) values for chosen parameter space for dye adsorption by GG/γ-$Fe_2O_3$

| **Dose ($gL^{-1}$)** | | **0.5** | **1** | **1.5** | **2** | **2.5** | **3** | | |
|---|---|---|---|---|---|---|---|---|---|
| | **CR** | 0.57518 | 0.72514 | 0.60069 | 0.57518 | 0.52452 | 0.45894 | | |
| | **NB** | 0.43035 | 0.32741 | 0.4 | 0.4 | 0.44576 | 0.50863 | | |
| **Concentration ($mgL^{-1}$)** | | **5** | **10** | **15** | **20** | **25** | **30** | | |
| | **CR** | 0.25007 | 0.7 | 0.19757 | 0.92738 | 1.10036 | 0.75 | | |
| | **NB** | 0.47085 | 0.50319 | 0.46184 | 0.0755 | 1.05057 | 0.71042 | | |
| **pH** | | **2** | **4** | **6** | **7** | **8** | **10** | **11** | |
| | **CR** | 0.07211 | 0.25239 | 0.91504 | 0.32512 | 0.12583 | 0.78307 | 0.91198 | |
| | **NB** | 0.39345 | 0.66091 | 1.11355 | 0.09 | 0.45 | 0.2623 | 0.40415 | |
| **Contact time (min)** | | **15** | **30** | **45** | **60** | **75** | **90** | **105** | **120** |
| | **CR** | 0.45 | 0.54 | 0.41 | 0.43 | 0.61 | 0.20421 | 0.5 | 0.38 |
| | **NB** | 0.34828 | 0.28844 | 0.22539 | 0.29462 | 0.4293 | 0.55973 | 0.66461 | 0.80467 |

**Table S4.** Statistical treatment using one-way ANOVA analysis of operational conditions for CR and NB adsorption by GG/γ-$Fe_2O_3$

| **Parameter** | **Degrees of Freedom (DF)** | | **Sum of Squares (SS)** | | **Mean Square (MS)** | | **F value** | | **Prob>F (P-value)** | |
|---|---|---|---|---|---|---|---|---|---|---|
| | **CR** | **NB** | **CR** | **NB** | **CR** | **NB** | **CR** | **NB** | **CR** | **NB** |
| Dosage | 5 | 5 | 1060.93574 | 2063.3058 | 212.18715 | 412.66116 | 625.89684 | 2314.42042 | 4.53281E-14 | 1.80951E-17 |
| Concentration | 5 | 5 | 10.56629 | 611.692 | 2.11326 | 122.3384 | 3.93177 | 318.82483 | 0.02416 | 2.52611E-12 |
| pH | 6 | 6 | 5760.22846 | 8326.02903 | 960.03808 | 1387.6715 | 2717.8581 | 4271.01005 | 1.22826E-20 | 5.20416E-22 |
| Contact time | 7 | 7 | 151.737 | 32.26886 | 21.67671 | 4.60984 | 104.76271 | 19.11903 | 3.65731E-12 | 1.17045E-6 |

**Table S5.** d-spacing calculated from TEM-SAED pattern of GG/γ-$Fe_2O_3$

| S.No. | 1/2r ($nm^{-1}$) | 1/r ($nm^{-1}$) | r (nm) | d-spacing | Miller indices (hkl) |
|---|---|---|---|---|---|
| 1. | 6.797 | 3.398 | 0.294 | 2.942 | (220) |
| 2. | 7.986 | 3.993 | 0.250 | 2.504 | (311) |

| | | | | | |
|---|---|---|---|---|---|
| 3. | 9.667 | 4.833 | 0.207 | 2.069 | (400) |
| 4. | 11.715 | 5.857 | 0.171 | 1.707 | (422) |
| 5. | 12.590 | 6.295 | 0.159 | 1.589 | (511) |
| 6. | 13.771 | 6.885 | 0.145 | 1.452 | (440) |

**Table S6.** MIC ($\mu gmL^{-1}$) and MBC ($\mu gmL^{-1}$) of GG and GG/γ-$Fe_2O_3$ against bacterial stains

| MIC & MBC ($\mu gmL^{-1}$) against tested bacterial strains | | *E. coli* | *S. aureus* |
|---|---|---|---|
| GG | MIC | 550.25 ±1.85 | 425.5 ± 1.25 |
| | MBC | 1100.5 ± 2.85 | 850.2 ± 1.85 |
| GG/γ-$Fe_2O_3$ | MIC | 250 ± 3.15 | 200 ± 2.62 |
| | MBC | 500 ± 1.98 | 400 ± 3.67 |

**Table S7.** MIC ($\mu gmL^{-1}$) and MFC ($\mu gmL^{-1}$) of GG and GG/γ-$Fe_2O_3$ against tested fungal strain

| MIC & MFC ($\mu gmL^{-1}$) against tested fungal strains | | *C. albicans (SC5314)* | *C. albicans (ATCC90028)* |
|---|---|---|---|
| GG | MIC | 300.85 ± 8.58 | 320.74 ± 5.65 |
| | MFC | 600.56 ± 7.56 | 645.32 ± 3.64 |
| GG/γ-$Fe_2O_3$ | MIC | 131.25 ± 2.56 | 125 ± 1.15 |
| | MFC | 465.5 ± 3.12 | 450 ± 2.30 |

**Table S8.** Parameters governing the mechanism of adsorption of CR and NB dyes on GG/γ-$Fe_2O_3$

| Pollutant | Intra-particle diffusion (Webber-Morris model) | | | Liquid film diffusion (Boyd model) | |
|---|---|---|---|---|---|
| | $k_{IPD}$ ($mgg^{-1}min^{-0.5}$) | C | $R^2$ | $k_{LFD}$ ($min^{-1}$) | $R^2$ |
| CR | 0.053 | 4.240 | 0.923 | 0.414 | 0.468 |
| NB | 0.049 | 9.178 | 0.919 | 0.030 | 0.946 |

**Table S9.** Removal of CR and NB dyes by GG/γ-$Fe_2O_3$ in real wastewater setup, and amidst competing ions

| **1. Real water analysis** | | | |
|---|---|---|---|
| **Type of water sample** | **% CR adsorption** | **% NB adsorption** | **% CR degradation** |
| Sewage water | 33.03 | 36.6 | 26.19 |
| Tap water | 57.84 | 44.18 | 42.85 |
| RO water | 91.81 | 89.55 | 54.79 |
| **Distilled water** | **97.51** | **91.38** | **92.7** |
| **2. Effect of co-existing ions** | | | |
| $NO_3^-$ | 95.6 | 90.45 | 74.29 |
| $Cl^-$ | 97.02 | 87.66 | 89.25 |
| $SO_4^{2-}$ | 94.34 | 82.72 | 64.63 |
| $CO_3^{2-}$ | 0.81 | 84.46 | 6.85 |
| $Na^+$ | 96.9 | 80.66 | 89.25 |
| $Ca^{2+}$ | 90.17 | 82.15 | 85.71 |

**Table S10.** Effect of dye mixtures on CR and NB adsorption by GG/γ-$Fe_2O_3$

| 10 $mg^{-1}$ Dye 1 (A) | 10 $mg^{-1}$ Dye 2 (A) | 20 $mg^{-1}$ Dye 3 (C) | 20 $mg^{-1}$ Dye 4 (C) | % CR adsorption | % NB adsorption |
|---|---|---|---|---|---|
| CR | - | - | - | 97.51 | - |
| - | - | NB | - | - | 91.38 |
| CR | - | NB | - | 85.44 | 86.99 |
| CR | EY | NB | NF | 67.88 | 87.37 |
| CR | DR-81 | NB | BB-R | 82.87 | 82.76 |
| CR | AR-S | NB | CV | 90.14 | 89.07 |
| CR | TB | NB | Ph | 84 | 73.26 |
| CR | ChR | NB | MG | 46.77 | 78.02 |

**Table S11.** Cost estimation for laboratory-scale synthesis of GG/γ-$Fe_2O_3$

| Breakup of cost | Amount per batch | Unit Cost | Cost (USD, $) | Remarks |
|---|---|---|---|---|
| *Glycyrrhiza glabra* root | 10 g | Negligible | $0/g | Locally sourced |
| $Fe(NO_3)_3.9H_2O$ | 2.02 g | $35.09/250 g | $0.28/g | ThermoFisher |
| $FeSO_4.7H_2O$ | 0.695 g | $43.91/250 g | $0.12/g | Merck |
| NaOH, Ethanol | Small | Estimate | $0.15 | Neutralisation/purification |
| Distilled water (DW) | ~1 L | Estimate | $0.06 | Lab-prepared |
| Energy | - | Estimate | $0.18-0.27 | For heating, drying, stirring |
| **Total (per batch)** | - | - | $0.79-0.88 | Lab-scale estimation |

**Table S12.** Cost of water treatment by GG/γ-$Fe_2O_3$ under optimized conditions

| Factor | Approx. Value | Cost Implication (USD, $) |
|---|---|---|
| GG/γ-$Fe_2O_3$ dose | 0.2 g $L^{-1}$ | $0.158–$0.176/L (*$158–$176/1000 L*) |
| Optimum adsorption time | 60 min | Feasible for batch adsorption setups |
| Sunlight-driven photodegradation | 160 min | None |
| pH Adjustment | pH=2-4 (CR); pH=11 (NB) | $0.012–$0.024 per 1000 L (Estimate) |
| Regeneration cycles | 4 cycles (practically feasible) | Recurring cost reduced by 70–80% |

**Table S13.** Comparative study of other adsorbents used for CR and NB removal

| Pollutant | Adsorbent | Dose ($gL^{-1}$) | Conc. ($mgL^{-1}$) | Time (min) | pH | Temp (°C) | Adsorption capacity ($mgg^{-1}$) | Reference |
|---|---|---|---|---|---|---|---|---|
| CR | Fly ash | 1 | 30 | 60 | - | 50 | 22.12 | [10] |
| | Zeolite | - | - | - | - | - | 8.1 | [11] |
| | *Padina gymnosphora* (PG) | - | - | - | - | - | 11.59 | |
| | Zeolite/algae composite (ZPG) | 1 | 20 | 480 | 7 | 25 | 11.26 | |
| | $SiO_2$-PDA-PTAC | 0.2 | 60 | 180 | 3 | 65 | 125 | [12] |

| | | | | | | | | |
|---|---|---|---|---|---|---|---|---|
| | $Cu/TiO_2$ | 1 | 20 | 10 | 6 | - | 46.49 | [13] |
| | $GO–MnFe_2O_4$ | 1 | 40 | 60 | - | - | 8.597 | [14] |
| | G-3PS | 1 | 22 | 30 | 5 | 40 | 14.82 | [15] |
| | G-5PS | | 22 | 20 | 5 | 40 | 16.04 | |
| | $GG/\gamma\text{-}Fe_2O_3$ | 0.2 | 10 | 60 | 2-4 | 50 | 47.504 | **Present Study** |
| NB | Ag-rGO | 0.5 | 20 | 60 | 6 | 30 | 6.685 | [16] |
| | RAM | - | - | - | - | - | 21.2 | [17] |
| | P(AAm-co-AcA) | 1.5 | - | - | - | - | 16.86 | [18] |
| | Natural clay | 4 | 500 | 480 | 5 | - | 25 | [19] |
| | $GG/\gamma\text{-}Fe_2O_3$ | 0.2 | 20 | 60 | 11 | 30 | 15.361 | **Present Study** |

**Table S14.** Comparative analysis of CR degradation efficiency with previously reported catalysts.

| **Photocatalyst** | **Dose ($gL^{-1}$)** | **Conc. ($mgL^{-1}$)** | **Time (min)** | **PFO rate Constant ($\times10^{-3}$ $min^{-1}$)** | **Light Source** | **% CR degradation** | **Reference** |
|---|---|---|---|---|---|---|---|
| $Co_3O_4/TiO_2/GO$ | 0.25 | 10 | 90 | 23.5 | Xe 300 W | 91 | [1] |
| CS/n-CdS | 1.5 | 20 | 180 | 11.08 | Xe 300 W | 86 | [2] |
| P25 $TiO_2$ | 1 | 40 | 210 | - | W 300W | 90 | [3] |
| Cu foam | - | 30 | 300 | 3.53 | Sunlight | 60 | [4] |
| CuO | | | | 5.01 | | 75 | |
| ZnO@CuO | | | | 7.12 | | 90 | |
| $Fe_3O_4$@CuO | | | | 7.95 | | 94 | |
| PAC | 2 | 50 | 1.5 | 1513.8 | Microwave | 87.79 | [5] |
| Iron promoted$TiO_2$AC NCs | 10 | $5 \times 10^{-5}$ M | 300 | 2.11-4.70 | Visible | 84.46 | [6] |
| Cellulose/$\gamma–Fe_2O_3–ZrO_2$ | 50 mg | 100 | 30 | 9.1 | Visible | 98.5 | [7] |
| $\alpha\text{-}Fe_2O_3$/rGO | 0.2 | 50 | 30 | 31.8 | Visible | 87 | [8] |
| $BaDy_xFe_{12-x}O_{19}$ | 0.3 | 10 | 90 | 19 | Sunlight | 89.29 | [9] |
| $GG/\gamma\text{-}Fe_2O_3$ | 0.2 | 10 | 160 | 14.00 | Sunlight | 92.7 | **Present Study** |

## References


1 W. K. Jo, S. Kumar, M. A. Isaacs, A. F. Lee and S. Karthikeyan, Cobalt promoted $TiO_2$/GO for the photocatalytic degradation of oxytetracycline and Congo Red, *Appl Catal B*, 2017, **201**, 159–168.

2 H. Zhu, R. Jiang, L. Xiao, Y. Chang, Y. Guan, X. Li and G. Zeng, Photocatalytic decolorization and degradation of Congo Red on innovative crosslinked chitosan/nano-CdS composite catalyst under visible light irradiation, *J Hazard Mater*, 2009, **169**, 933–940.

3 H. X. Guo, K. L. Lin, Z. S. Zheng, F. Bin Xiao and S. X. Li, Sulfanilic acid-modified $P_{25}$ $TiO_2$ nanoparticles with improved photocatalytic degradation on Congo red under visible light, *Dyes and Pigments*, 2012, **92**, 1278–1284.

4 D. Malwal and P. Gopinath, Enhanced photocatalytic activity of hierarchical three-dimensional metal oxide@CuO nanostructures towards the degradation of Congo red dye under solar radiation, *Catal Sci Technol*, 2016, **6**, 4458–4472.

5 Z. Zhang, Y. Shan, J. Wang, H. Ling, S. Zang, W. Gao, Z. Zhao and H. Zhang, Investigation on the rapid degradation of congo red catalyzed by activated carbon powder under microwave irradiation, *J Hazard Mater*, 2007, **147**, 325–333.

6 D. Negoescu, V. Bratan, M. Gherendi, I. Atkinson, D. C. Culita, A. Neacsu, A. Baran, S. Petrescu and V. Parvulescu, Iron Promoted $TiO_2$-Activated Carbon Nanocomposites for Photocatalytic Degradation of Congo Red in Water, *Catalysts*, 2024, **14**, 844.

7 H. Helmiyati, N. Fitriana, M. L. Chaerani and F. W. Dini, Green hybrid photocatalyst containing cellulose and $\gamma$–$Fe_2O_3$–$ZrO_2$ heterojunction for improved visible-light driven degradation of Congo red, *Opt Mater (Amst)*, 2022, **124**, 111982.

8 Y. Wang, S. Wang, Y. Wu, Z. Wang, H. Zhang, Z. Cao, J. He, W. Li, Z. Yang, L. Zheng, D. Feng, P. Pan, J. Bi, H. Li, J. Zhao and K. Zhang, A $\alpha$-$Fe_2O_3$/rGO magnetic photocatalyst: Enhanced photocatalytic performance regulated by magnetic field, *J Alloys Compd*, 2021, **851**, 156733.

9 Himanshi, J. Makasana, S. Ganesan, B. Lal, K. S. Naidu, J. Ahmed, J. Prakash, A. Verma, N. Lakshmaiya, R. Jasrotia, X. Yong and C. K. Chan, Insights into the enhanced photocatalytic degradation of congo red using advanced $BaD_{yx}Fe_{12-x}O_{19}$ catalytic hexamaterials, *Sci Rep*, 2025, **15**, 1–20.

10 M. Harja, G. Buema and D. Bucur, Recent advances in removal of Congo Red dye by adsorption using an industrial waste, *Sci Rep*, 2022, **12**, 1–18.

11 A. R. Dryaz, M. Shaban, H. AlMohamadi, K. A. A. Al-Ola, A. Hamd, N. K. Soliman and S. A. Ahmed, Design, characterization, and adsorption properties of Padina gymnospora/zeolite nanocomposite for Congo red dye removal from wastewater, *Sci Rep*, *2021*, **11**, 21058.

12 J. Zhu, K. Wang, S. Fan, A. Ouyang, J. Gu, J. Tian, M. Liu, F. Deng, X. Zhang and Y. Wei, Preparation of $SiO_2$ composites for efficient removal of Congo red via the combination of mussel-inspired surface modification and anionic ring-opening polymerization, *Colloids and Surfaces C: Environmental Aspects*, 2025, **3**, 100078.

13 S. Zhang, Q. Luo, X. Sun, L. Chi, P. Sun and L. Zhang, Facile synthesis copper-modified titania (Cu/$TiO_2$) nanoparticles for high-efficiency Congo red adsorption, *Chin J Chem Eng*, 2025, **81**, 87–94.

14 A. Zourou, A. Ntziouni, N. D. Adamopoulos, T. Roman, F. Zhang, M. Terrones and K. V. Kordatos, Graphene oxide–$MnFe_2O_4$ nanohybrid material as an adsorbent of Congo red dye, *Journal of Physics and Chemistry of Solids*, 2023, **181**, 111490.

15 A. Ebelegi, N. Ayawei and D. Wankasi, Efficient Sequestration of Congo Red Dye From Aqueous Solutions Using Pamam Dendrimer – Silica Composite, *Water Air Soil Pollut*, 2024, **235**, 1–15.

16 N. Natasha, A. Khan, U. U. Rahman, N. Sadaf, M. Yaseen, R. A. Abumousa, R. Khattak, N. Rehman, M. Bououdina and M. Humayun, Effective Removal of Nile Blue Dye from Wastewater using Silver-Decorated Reduced Graphene Oxide, *ACS Omega*, 2024, **9**, 19461–19480.
17 G. Güçlü, Removal of basic dyes from aqueous solutions by dimethyl terephthalate distillation residue, *Desalination*, 2010, **259**, 53–58.
18 Y. Işikver, Removal of some cationic dyes from aqueous solution by acrylamide- or 2-hydroxyethyl methacrylate-based copolymeric hydrogels, *Fibers and Polymers*, 2017, **18**, 2070–2078.
19 T. B. Iyim and G. Güçlü, Removal of basic dyes from aqueous solutions using natural clay, *Desalination*, 2009, **249**, 1377–1379.